The origins and variation of terrestrial ENA outflow

G. R. Wilson
Mission Research Corporation, Nashua, NH

T. E. Moore
Goddard Space Flight Center, Greenbelt, MD

Abstract

Analysis of ENA data from the LENA instrument on the IMAGE spacecraft shows that the terrestrial atmosphere is a copious emitter of energetic neutral atoms (< 300 eV) under all conditions. When activity is low the observed emissions are concentrated close to the earth and are presumed to be the high energy tail of the warm oxygen geocorona, with energies < 2 eV. When activity increases the relative abundance of the higher energy neutrals increases and the emissions can be seen farther from the earth. Because of the close correlation between the post-perigee ENA flux (fluxes seen 1-2 hours after spacecraft perigee) and Ap, and the fact that the post-perigee fluxes are seen when no magnetic storm is in progress, we conclude that many of the emitted ENA come from the auroral zone and are produced by energized ionospheric ions rather than by precipitating energetic ions. In more spectacular events such as the Bastille Day storm event (July 14-16, 2000), oxygen neutral emissions produced by precipitation of keV ring current oxygen ions can also make an important contribution to the total neutral emission. We conclude that diurnal variation in ENA emissions is a winter hemisphere feature that is absent in the summer hemisphere. As activity increases, the altitude range of the auroral oval ENA emission region increases.

1. Introduction

With the launch of the IMAGE spacecraft [*Burch*, 2000] on 25 March 2000 the dream of doing routine ENA imaging of magnetospheric plasmas became a reality. In addition to an instrument designed to look at the ENA energy range of traditional interest (10-300 keV) [*Mitchell et al.*, 2000] the spacecraft carried two instruments designed to image lower energy neutrals. The LENA instrument [*Moore et al.*, 2000] was designed to image oxygen and hydrogen neutrals in the energy range of 10-300 eV. A preliminary report on the data from that instrument [*Moore et al.*, 2001] described the presence of intense neutral fluxes seen by the LENA instrument when the IMAGE spacecraft passed through perigee. In a previous paper [*Wilson et al.*, 2003] we presented our introductory detailed analysis of the perigee pass data collected by the LENA instrument during the summer of 2000.

In this paper we return to our analysis of the LENA perigee data collected during the summer of 2000 and expand the discussion to include ENA emissions seen by LENA at other points in its orbit away from perigee. We include new data that were not available when the previous analysis was done, and compare it against a model of ENA emission designed to assist in the analysis.

Because of the novelty of the LENA measurements and the lack of previous experience with this type of instrument it is necessary to proceed carefully and with a full understanding of the limitations of the LENA imager. Our goal is to establish a clear understanding of the low energy ENA emanating from the earth and the process or processes responsible for its production. One obstacle to achieving this goal is the fact that the instrument achieved less then the hoped for resolution because of scattering at the conversion surface. In this study we analyze the data in such a way so as to minimize the contribution of this lack of resolution while demonstrating how the data respond to changing geophysical conditions.

The LENA instrument was designed to resolve the angle of arrival (8 deg x 8 deg pixels), energy (10—300 eV in 3 pixels of 100% width), and composition (H or O) of incoming ENA. The instrument has a fan shaped, instantaneous field-of view of 8º×90º, which sweeps through 360º as the spacecraft spins (2 min period). In practice, owing to scattering from the conversion surface, the resolved polar angle pixels were approximately 20 deg. wide. This is insufficient to resolve the auroral features of interest, so we sum over the reported polar angle. The energy resolution is also insufficient to resolve auroral beam distributions, so we average over this reported quantity as well. The composition of the incoming ENA is also ambiguous because of sputtering at the charge conversion surface. Preflight test showed that low energy oxygen ENA (10—300 eV) sputtered significant amounts of low energy negative hydrogen ions off the conversion surface. The reverse was not true for hydrogen. However, higher energy hydrogen ENA (> 400 eV) could sputter significant quantities of low energy (10—300 eV) negative oxygen ions from the conversion surface. Since the composition information could not be used at face value we ignore it here. Another issue is that the response of the instrument for low energy oxygen ENA (< 30 eV) was never tested so that we do not know how the oxygen low energy cutoff behaves. The instrument response for low energy hydrogen ENA (10—30 eV) was tested and we know that the instrument response drops very rapidly below 15 eV. Issues of the response of the instrument to ultraviolet light and energetic ions or electrons were discussed in our previous paper [*Wilson et al.*, 2003].

There are three main processes which are responsible for producing ENA near the earth that would be visible to the LENA instrument (have energies above ~10 eV and less than 1 keV in the spacecraft frame). The first of these is the energization of ionospheric ions followed by their

charge exchange with neutral atoms in the thermosphere (H, O, He) or geocorona (H). The second comes from precipitating magnetospheric ions which can produce low energy ENA by two routes. The first is through the so-called ENA mirroring process of *Galand and Richmond* [1999] where precipitating ions, through a series of charge exchange and charge stripping reactions, end up being sent upward again with an energy below the ion's original energy. The second route is the so-called oxygen backsplash process of *Ishimoto et al.* [1992] where precipitating energetic oxygen ions eject low energy oxygen atoms and N_2 molecules from the thermosphere. The third process for producing low energy ENA near the Earth, consists of a set of exothermic reactions that produce oxygen atoms with energies of 1 to 5 eV [*Hickey et al.*, 1995]. These lower energy oxygen neutrals could be visible to the LENA instrument when their energy in the spacecraft frame is boosted by the ram effect.

The first two of the ENA production processes discussed above will be closely associated with the auroral oval while the last one will be most prolific on the day side of the earth. The goal of our analysis of the LENA data is to answer the following two questions:

1. What are the near Earth source regions of low energy ENA?
2. Do the low energy ENA emissions vary with geophysical conditions in a way consistent with known geophysical processes?

2. The July 13, 2000 Events

In figure 1 we show the LENA data from two consecutive perigee passes that occurred on July 13, 2000. The format of these spectrograms is the same as those shown in *Wilson et al.* [2003]. Each vertical band represents a single image that has been collapsed over mass, energy and polar angle so that it only gives coincident counts versus spacecraft spin phase. Each image is collected over 2 min (spacecraft spin period) and there are 70 images in each panel covering a total time interval of 140 min. The lines over plotted in each panel represent nadir (dotted), trailing and approaching limbs of the earth (dashed-dotted), and the ram (dashed) directions. The approaching limb is the lower of the two dash-dotted curves and is the limb of the earth toward which the spacecraft is moving. The trailing limb is dash-dotted curve furthest from the ram direction. The data in each of these two passes have had radiation belt background removed by subtraction of a Gaussian fit to the background counts from the radiation belt. The spacecraft spin axis is perpendicular to the orbit plane so the LENA instantaneous field-of-view straddles the orbit plane. Since the data is collapsed over the polar angle images become one dimensional functions of spacecraft spin angle only. The nadir, limb and ram directions marked in figure 1 correspond to the point in spin phase when the center of the instantaneous field-of-view points in those directions. For the time interval of the data used in this paper the spacecraft perigee (1000 km) was in the southern hemisphere at about -50º geographic latitude and the orbit plane was primarily dawn-dusk.

Panel (a) of figure 1 shows data from the first perigee pass on the 13th that began late on the 12th of July. Perigee was reached at 0010 UT on the 13th. Panel (b) shows the data from the second pass which reached perigee at 1424 UT on the 13th. The first thing to notice in comparing these two passes is that the second pass is brighter overall than the first. But what is more instructive is to notice where the second pass is brighter. In both of these passes perigee occurs at mid magnetic latitudes; -42º for the first and -54º for the second. To the left of these points in each panel the second pass is much brighter than the first. In the second pass one sees much higher fluxes coming from the earth when the spacecraft is at high magnetic latitudes over the southern magnetic pole.

The second place where the second pass is brighter than the first is in fluxes seen coming from beyond (above) the trailing limb. In our previous analysis [*Wilson et al.*, 2003] we showed that such neutrals (assuming oxygen) must have energies above about 30 eV and are on escaping hyperbolic trajectories. Such neutrals would have their velocities little deflected by gravity and would therefore be traveling in nearly straight lines. If the observed neutrals are hydrogen the straight line assumption is even easier to demonstrate. The observation then of fluxes coming from points well above the trailing limb indicates a source region that is well above the earth's surface. This source region is more active during the second pass than the first.

The third difference between the two passes is the fluxes seen coming from the direction of the earth that can be seen clearly in panel (b) after about 1515 UT. Although such fluxes are weak compared to what is seen earlier in the pass they are clearly there and they are absent (at that level) from the first pass in panel (a).

The natural question to ask is what changed between the times of these two passes. In our previous paper [*Wilson et al.*, 2003] we noted that there is a strong diurnal variation in the over all intensity of perigee pass emissions. The variation is sinusoidal with a peak at 0740 UT and a minimum 12 hours later. The two perigee passes from July 13th occur at nearly symmetric times on either side of the diurnal peak so this variation cannot account for the differences seen in figure 1.

The main reason for the differences between panels (a) and (b) in figure 1 is a change in activity level that occurred during the intervening 14 hours. Figure 2 shows the Kan-Lee electric field [*Kan and Lee*, 1979] and the solar wind dynamic pressure from ACE data that have been time shifted to give its arrival time at X (GSM) = 0. The vertical dashed lines (labeled (a) and (b)) give the times of the two perigee passes. Clearly there was a large increase in the energy input to the magnetosphere between the two passes. At the time of the first pass Kp was 1 while during the second it was 7. The increase in energy input, however, did not lead to the onset of a large magnetic storm. The IMF did not remain consistently southward after the shock arrival and, all though the IMF B_Z was mostly positive before the shock arrived at 0950 UT, the plasma sheet was not likely loaded with high densities because the pre-shock solar wind density was not very high ($\leq$ 5 cm^{-3}) [*Thomsen et al.*, 2003]. At the time of the first pass Dst was -7 nT and at the time of the second pass it was -10 nT. The pressure pulse that arrived just after 1000 UT lead to a jump in Dst to 50 nT for 10-11 UT. Dst dropped later in the day to a minimum -43 nT (21-22 UT) before recovering. It is safe to assume that the ring current was not burgeoning with energetic oxygen ions at the time of the second perigee pass on July 13th.

In conclusion then we can say that with the increase in magnetic activity came an increase in the neutral emissions from the high latitude atmosphere and from regions well above the trailing limb. The assumption is that this indicates the presence of more energetic neutrals which is confirmed by the fluxes seen coming from the earth while the IMAGE spacecraft was climbing to high altitudes over the northern hemisphere. Two processes have been proposed to be the source for these energetic neutrals: (1) ion energization in the auroral zone, and (2) ENA backsplash generated by precipitating, energetic hydrogen or oxygen ions. Because of the weakness of the ring current at the time of the second pass it is unlikely that oxygen ion precipitation made a significant contribution to the emissions seen in the second pass. Hydrogen ion precipitation, however, may have made a contribution to those emissions.

Another thing to conclude from this example is that the intense fluxes seen after perigee and between the nadir and ram directions that are common to both passes represents the quiet time signal. Their positioning between the nadir and ram directions indicates that they are lower energy

particles. Modeling results, based on the model presented by Wilson et al. [2003] will be shown later in this paper, supporting the idea that these are part of the hot oxygen geocorona.

3. The Bastille Day Storm (July 15-16, 2000) Event

Figures 3 and 4 show data from one of the most spectacular events seen in the LENA data set that occurred during the Bastille Day storm. Figure 3 is another spin-time spectrogram with the same format as used in figure 1. For these data radiation belt background was removed in the same fashion as was done for figure 1. Perigee time was 2320 UT.

As with the second perigee pass of July 13th one sees intense fluxes coming from the earth while IMAGE is at high latitudes (before 2320 UT). Also seen near perigee are large fluxes coming from beyond the trailing limb and intense fluxes from the earth while IMAGE is climbing over the northern polar regions. In all cases though, the fluxes are larger than the July 13th case. This should not come as a surprise in view of the fact that Kp was 9- changing to 8- during the time interval of figure 3. This time interval occurred during the main phase of the Bastille Day storm when Dst was -281 to -301 nT.

Another thing to note is the pattern made by the high latitude emissions seen coming from the earth between 2250 and 2318 UT. At first emissions are brightest near the approaching limb. As the spacecraft climbs to higher latitudes the emissions spread out across the entire earth and then split into two branches, one that angles up toward the trailing limb and one that follows the approaching limb. Later the two branches rejoin and the emissions again spread across the whole face of the earth. This changing pattern of the emissions is very similar to what is seen in figure 9 of *Wilson et al.* [2003]. In that figure a model was used to simulate what emissions coming from a hypothetical auroral oval between 60º and 75º magnetic-latitude would look like to the LENA instrument. As the spacecraft approaches the auroral oval from low latitudes emissions are first seen on the approaching limb. This pattern spreads out toward the trailing limb and covers the earth when the spacecraft flies over the aurora. As the spacecraft moves over the polar cap the emissions split into two branches which later recombine when the spacecraft flies over the other side of the aurora.

We note at this point that the emission pattern seen in figure 3 between 2250 and 2318 UT is atypical. The Bastille Day storm event is the only example like it that we have found so far among the perigee pass data that we have examined (June to August 2000). That may very well be due to the fact that in terms of the level of magnetic activity this was a unique time interval. We have examined Polar UVI auroral images for many of the perigee passes that occurred in the summer of 2000 and found that the auroral oval at the time of the Bastille Day storm perigee pass was unique in terms of the intensity of the aurora and the size of the auroral oval. Figure 4 shows an average auroral image made by averaging the 60 UVI LBHL images taken between 2250 and 2326 UT on July 15th. As can be seen in that figure the center of the auroral oval, at least in the post-midnight and dawn sectors, is at about 60º magnetic latitude. The auroral oval in the dusk sector extends outside the field-of-view of the camera. UVI images taken at times earlier than 2250 UT show intense emissions coming from the dusk side of the auroral oval which drop out of the field-of-view of the instrument as Polar moves in toward perigee.

The upshot of this example is that intense neutral emissions are again seen in those three key areas (earth centered at high southern latitudes, beyond the trailing limb, and earth centered at high northern latitudes from large geocentric distances) but this time with greater intensity compared to the second July 13th event. Also seen is the emission pattern of the auroral oval that is not seen in

any other case. Possibly processes (collisions?) act to smear out or obscure the auroral oval pattern when the auroral oval is smaller and the emission are weaker or less energetic. Also, the pattern could be obscured by an auroral oval that did not uniformly emit ENA from all local time sectors.

4. Relationship of the post-perigee signal to the perigee signal and magnetic activity

To begin we return here to something illustrated by figure 1. One can see that the images collected while the spacecraft was at high latitudes (before perigee) are significantly brighter in the second perigee pass than the first. The images taken after perigee are comparable in intensity for both passes. This suggests that there is a different type of behavior between these two sets of images and that the fluxes seen in the high latitude images are more responsive to magnetic activity. In view of this we have gone back to the perigee pass data presented in *Wilson et al.* [2003] and split the images from each perigee pass into two groups. The break point for this split was typically near -55º MLat when IMAGE was close to perigee. The high latitude portion of the perigee pass is then the 5-8 images taken at magnetic latitudes ≤ -55º before perigee while the low latitude portion is only the 4 images taken at magnetic latitudes ≥ -55º immediately after perigee. The low latitude portion was restricted to 4 images to avoid any contribution to the signal from the radiation belt. Splitting the perigee signal this ways makes sense from a geophysical perspective. For the high latitude images the spacecraft is in an ideal position to look down on the auroral zone and polar cap while for the low latitude images it is not. Furthermore, at high latitudes the spacecraft is low enough to be in the source region if it extends above 1000 km.

Figure 5 plots the integrated flux (counts converted to flux and integrated over polar angle, spin angle, energy and mass and summed over all images) for the high latitude and low latitude portions from 57 perigee passes that occurred between 10 June and 30 July 2000. In the top two panels points marked with an open square are passes for which Kp was 4+ or less. Points marked with a filled square had a Kp ≥ 5-. Each filled point is marked with its value of Kp. The sinusoidal curves in each panel of figure 5 were fit to the Kp ≤ 4+ data. One notes in the top two plots that the diurnal variation apparent in figure 5 from *Wilson et al.* [2003] is also apparent here but more closely represents the variation among the high latitude images than the low latitude ones. Also note that the sinusoid peaks near 0900 UT for the high latitude images and near 0700 UT for the low latitude images. This is to be compared to a sinusoidal peak of 0740 UT when the high and low latitude images are combined.

The bottom two panels of figure 5 demonstrate how well the two sets of integrated fluxes correlate with magnetic activity. Before plotting the points the diurnal variation was removed by subtracting the sinusoidal curves for the respective data sets. As can be seen from these two plots the integrated intensity of the high latitude images is better correlated with magnetic activity than the integrated intensity of the low latitude images. The initial impression from figure 1 is substantiated in this statistical analysis.

Now that we have seen how the two parts of the perigee data vary with UT and Ap the next question to ask is how the post-perigee signal correlates with the perigee pass signals discussed above. To answer that question we first quantified the post-perigee signal. To do this we took LENA data from 67 orbits that occurred between 10 June and 30 July, 2000 for which the background was not high enough to obscure the signal. We then took the first 30 images that were obtained in a time interval that started one hour after perigee and summed up all of the coincident counts as a function of spin phase. Typically the integration time interval spanned one hour but in some cases extended to two hours because of missing images. We did this integration to bring out

the intensity of the post-perigee signal for the weaker events. For the post-perigee signal the spacecraft was at high magnetic latitudes at geocentric distances of 3-5 R_E. This is again an ideal position from which to observe the auroral zone and polar cap, but from a greater distance. The end result was a set of 67 plots of integrated counts versus spin phase. In these plots the primary features were the sun pulse and a peak centered on, or near the earth. The degree to which the counts went to zero between these two peaks was taken as a measure of the background level which we subtracted from the earth peak to get the post-perigee earth signal strength. The final value for the post-perigee signal was found by summing the background corrected counts in the 5 spin angle bins (15-19) centered on the nadir direction (bin 17).

Among the 67 orbits for which it was possible to obtain a post-perigee signal only 48 had a useable corresponding perigee signal (images from the perigee pass that preceded the post-perigee signal data interval.) In figure 6 we show two plots where these 48 post- perigee signals are plotted versus the (a) high latitude and (b) low latitude portions of the corresponding perigee pass signal. Each of the perigee pass values was corrected for diurnal variation by subtracting the value of the corresponding sinusoidal curve at the given UT. In each panel a line is fit to the data and the correlation coefficient is shown for each data set. Clearly the strength of the post-perigee signal is better correlated with the intensity of the high latitude portion of the perigee pass signal than with the low latitude portion. This behavior, apparent in figure 1, is fairly common in the data.

Given that the high latitude portion of the perigee pass data are well correlated with magnetic activity and with the post-perigee signal it stands to reason that the post-perigee signal will correlate well with magnetic activity. Figure 7 is a plot of the post-perigee signal strengths versus the value of Ap at the time the data were collected. The dashed curve in the plot is a quadratic function (in log-log space) fitted to the data. The correlation coefficient between the two quantities plotted in figure 7 is 0.821. Clearly there is a trend of increasing post-perigee signal strength with increasing magnetic activity. The high value point near the end of the fitted line is the Bastille Day event discussed above.

The diurnal variation apparent in both the high and low latitude portions of the perigee signal (figure 5) is not seen in the post-perigee signal.

5. Modeling Results

To understand the relationship between the intensity of the LENA signal seen at perigee and post-perigee, and the intensity and temperature of various source populations we present model results here. The model used is the same one used in *Wilson et al.* [2003]. It performs line of sight integrations along ENA orbital paths assuming that the observed neutrals are oxygen. It builds up a spin-time spectrogram like those seen in figures 1 and 3 by performing a double integration for each pixel of the spectrogram. The integrations are over the polar angle (fan direction) of the instrument's instantaneous field-of-view and the energy range of the instrument (10-300 eV). Flux is received at the spacecraft if the ENA's orbit tracked back from the spacecraft intersects the source region. Each contribution is weighted by the value of the oxygen ENA energy distribution at the point in the source region that the orbit tracks back to. To perform these simulations we used the IMAGE spacecraft ephemeris from the second perigee pass of July 13, 2000. The model makes no assumptions about what produces the ENA but is designed merely to illustrate how changing the source region or changing the energies of the source ENA changes the pattern seen in the reduced LENA data. The model is limited in that it is not time-dependent and can only easily handle source regions with simple geometries.

Figure 8 shows the results for four cases done with the model. In the first case the source region covered the entire surface of the earth below an altitude of 950 km. In this region there is a neutral oxygen population with a Maxwellian energy distribution that has a temperature of 2 eV. The density of this population is not specified and the resulting spin-time spectrogram is renormalized to have a peak count rate of 2000. In the subsequent cases in figure 7 we introduce an auroral oval which is a northern and southern annular ring centered at 65º magnetic latitude with an e-folding drop-off distance of 20º. The only thing different about the auroral oval is that the oxygen neutral temperature is higher than the surrounding atmosphere. The temperature of the oxygen atoms increases exponentially from a background value to some peak value at 65º. For the second case in figure 7 the background temperature is 2 eV and the peak auroral oval temperature is 5 eV. For the third case background *To* is 2 eV and the auroral oval peak *To* is 15 eV. For the last case these temperatures are 2 and 50 eV respectively.

The 2 eV background population is meant to simulate the chemically produced hot oxygen geocorona which can be approximated by a Maxwellian with a temperature near 2 eV [*Shematovich et al.*, 1994]. The increasing temperature in the auroral oval is meant to describe the likely increase in the hot oxygen energy distribution that would occur there due to auroral energy precipitation. In panel (a) of figure 8 one can see that most of the emissions are seen near the earth and are concentrated near the ram direction. These neutrals are visible to the instrument primarily because of the increased energy they have in the spacecraft frame of reference due to the motion of the spacecraft.

In the three following cases in figure 8 we see the effect of an increasing oxygen neutral temperature in the auroral zone. Note that the emissions seen coming from the earth in the post-perigee portion of the pass increase as the neutral temperature in the auroral oval increases. Also note that for the same changes in temperature the emissions seen near perigee spread toward the trailing limb and cover a greater portion of the earth. In the parlance of the previous section, the high latitude perigee signal and the post-perigee signal intensify together when the auroral oval neutral oxygen temperature increases. Because of the way each spectrogram is renormalized and because the model assumes an equal source density everywhere, as the auroral oval temperature increases the auroral oval population comes to dominate the hot oxygen population in its contribution to the spectrograms. This can be seen in the way the emissions centered on the ram direction tend to diminish in intensity relative to other regions in the spectrograms. If the model assumed different source densities for the hot oxygen neutrals relative to the heated auroral oval oxygen neutrals then this relative diminishing of the hot oxygen contribution need not occur. It would be possible, with the right combination of densities, to produce a spectrogram that is a blended form of panel 8(a) and 8(d) for example.

Note in the various cases in figure 8 that emissions are not seen very far behind the trailing limb as they are in figures 1 and 3. This is due mainly to the altitude cap of 950 km assumed for the source region in the model.

6. Evidence of High Altitude Auroral Zone Emissions

In many of the perigee passes large neutral fluxes are seen coming from spin directions that are beyond the trailing limb of the earth. Based on the analysis that was done in our previous paper [*Wilson et al.*, 2003] we know that the minimum energy of ENA detected by the instrument increases as the spin angle moves away from the ram direction. This results because at look directions away from the ram direction the ENA needs a larger velocity for its energy in the

spacecraft frame to be above the instrument detection threshold. Assuming oxygen neutrals and an instrument cutoff of 10 eV means that oxygen ENA seen coming from beyond the trailing limb have energies greater than 20-30 eV. That means these neutrals are traveling along fairly straight paths (little gravitational deflection) and their points of origin lie well above the earth's surface. (Note: even if we assume the observed ENA is predominately hydrogen the result that the source lies above the earth's surface still holds.) One might suspect that these ENA originate from a more distant source region like the ring current or the plasma sheet. In all of the perigee passes from 10 June to 30 July 2000 the emissions seen beyond the trailing limb are seen in only one, or at most two, consecutive images in the perigee pass. The sudden appearance and disappearance of this signal suggests that it comes from a small region that is close to the spacecraft. In most cases these emissions are seen when IMAGE is at high magnetic latitude and they tend to be seen more often when magnetic activity is high rather than low. Our interpretation of these emissions are that they come from the high altitude extension of the auroral oval and appear at spin phases away from the earth because the spacecraft is inside (or very close to) the source region and looking out through it [see also *Khan et al.*, 2003; for evidence of high altitude emissions].

To begin, note the images in figure 3 between 2250 and 2318 UT. In the first few images the emissions are strongest between the nadir and approaching limb directions. In subsequent images the intense emission region spreads until it covers the earth at which point emissions extend beyond the limb of the earth. In the four images after 2302 UT the emissions from beyond the limbs diminish while the main emissions from the earth split into two branches that track the two limbs. At 2310 UT the emissions again cover the earth and extend beyond the limb. This pattern (emissions beginning near the approaching limb, spreading across the earth, splitting into two branches and spreading across the earth again) is a signature of passage over the auroral oval and an example of it can be seen in figure 8(d). The points where the emissions spread over the earth are the places where the spacecraft is above the aurora. We can then conclude that in the places where the emissions are seen to come from beyond the trailing limb in the first part of figure 3 is where the spacecraft is passing over the auroral oval. On the dawn side the three images with trans-limb emissions are taken while the spacecraft is near 0500 MLT between -60º and -70º MLat. This is roughly consistent with where the auroral oval is at this time as shown in figure 4.

As another example, note the 7 image stripes in figure 1(b) between 1408 and 1422 UT. In the first two of these images one can see that the emissions extend somewhat beyond the trailing limb. In the next three images the emissions are confined mainly within the earth limbs and then in the final two images the emissions extend well beyond the tailing limb, much more then in the first images. During this time interval the spacecraft climbs from -48º MLat to -80º MLat and then drops to -62º MLat. The spacecraft drops in altitude from about 4400 km to 1250 km during the same time. We can interpret the pattern seen in the emissions as evidence that the neutral emission region extends to higher altitudes over the auroral oval than at other locations. When the first two images are taken the spacecraft is at an altitude of about 4000 km when it may be flying over the dawn side of the auroral oval. The emission region extends to higher altitudes than in the regions on either side but does not extend much above the altitude of the spacecraft. During the middle three images the spacecraft is passing over the polar cap and is outside of any source region. During the final two images the spacecraft again encounters the auroral region, but at a much lower altitude (1300-1500 km), and emissions are seen at much greater distances from the limb.

The behavior seen in these two examples is not seen in the first perigee pass on July 13th (figure 1(a)) during a very quiet interval. Apparently for the emission region to extend to high altitudes over the auroral oval active conditions are needed. We identified 20 perigee passes in the

June-July 2000 data set in which emissions where seen coming from beyond the trailing limb. The average value of the Kp index at the time of those passes was 5.

7. Discussion

In our previous paper [*Wilson et al.*, 2003] we argued that most of the perigee pass neutrals seen by LENA are oxygen. There are three possible mechanisms by which energetic oxygen neutrals (> 1 eV) can be produced near the earth. These are (1) exothermic reactions in the lower ionosphere/thermosphere [*Hickey et al.*, 1995], (2) charge exchange and energy degradation of precipitating energetic oxygen ions [*Ishimoto et al.*, 1992; *Bisikalo et al.*, 1995], and (3) charge exchange of energized, outflowing oxygen ions. Process 1 would be operating all of the time and should always be apparent in the data. Because these neutrals would have low energies (< 5 eV) they should only be seen near the earth when the LENA instrument is looking in and near the ram direction. Processes 2 and 3 will make much more variable contributions to the data but they will also produce more energetic oxygen neutrals than would be visible farther away from the earth and at directions away from ram. If most of the precipitating energetic oxygen ions come from the ring current then process 2 should be prominent mainly during the main phase of large magnetic storms.

The low latitude portion of the perigee pass data seems to be an ideal candidate to associate with process 1. It is always seen near perigee with large fluxes near the ram direction. Its dependence on magnetic activity is weaker than other parts of the LENA data and it has some dependence on solar activity (correlation coefficient of 0.42 with F10.7). There are however, two main problems with this interpretation. One is the broad spin angle extent of the emissions seen in these images. Our previous analysis [*Wilson et al.*, 2003] showed that oxygen neutrals seen more than 60º away from the ram direction have energies of 10 eV or greater. These would be inconsistent with process 1 and likely visible at greater distances from the earth than the data demonstrate. The other problem is the diurnal variation in the low latitude perigee signal. It is difficult to imagine how magnetic longitude sector could influence the hot oxygen production rate.

An alternate interpretation of the low latitude perigee signal is that it consists of low to medium energy (5-30 eV) oxygen neutrals produced in and near the cusp region. This would account for the diurnal variation in the signal. The draw back to this interpretation is explaining how these cusp produced neutrals can be seen at latitudes well away from the cusp coming from directions (even with ram and gravitational deflection considered) that don't map back to the cusp.

The post-perigee signal and the high latitude perigee signal appear to be closely associated with processes 2 and/or 3. They are sensitive to magnetic activity and their correlation with each other and their similarity with the modeling results suggests that the auroral oval is their main source. The ion outflow results of *Yau et al.* [1988] and *Peterson et al.* [2001] show that the oxygen ion outflow rate increases by a factor of 20-25 when Kp increases from 0 to 6. The results in figure 7 show an average increase in the post-perigee signal intensity of about a factor of 20 when Ap increases from 2 (Kp = 0+) to 80 (Kp = 6). As with any ENA signal the intensity depends on ion fluxes and neutral densities (either of which can be highly variable in this situation), but the similarity between the variation in the O^+ outflow rate and the post-perigee signal intensity suggests that process 2 is the important one in this case.

The correlation between the high latitude perigee pass signal and the post-perigee signal is best when the diurnal variation of the high latitude perigee pass signal is removed. This diurnal variability is one thing that the two signals do not share. Why does the post-perigee signal lack a diurnal variation?

One possibility is that the lower energy oxygen neutrals emitted from the auroral oval vary diurnally while the higher energy neutrals (those that reach the spacecraft at higher altitudes) do not. If this were the case the high latitude perigee images should show a diurnal variation in brightness for spin angles close to ram but no diurnal variation at spin angles away from ram. Such is not the case. The diurnal dimming and brightening of the high latitude perigee images extends across all spin angles.

We argued previously [*Wilson et al.*, 2003] that the diurnal variation of the perigee signal is due to the sunward and anti sunward motion of the auroral oval. One thing that distinguishes the high latitude perigee signal from the post-perigee signal is that they originate in different hemispheres. The high latitude perigee signal comes from the southern hemisphere auroral zone while the post-perigee signal comes from the northern hemisphere auroral zone. In the June-July time interval of interest the southern high latitude region receives little sun light while the northern high latitude region is well illuminated. If the diurnal variation in the southern hemisphere signal is due to the sunward/anti-sunward motion of the dayside auroral oval then the lack of a diurnal variation in the northern hemisphere signal may be due to the more uniform conditions experienced by the dayside northern auroral oval in its daily motions.

One should note in figure 5 that the diurnal variation in the high latitude perigee signal is very apparent in the quite time passes. This is consistent with the idea that under such conditions most escaping oxygen ions (and ENA) produced in the auroral zone come from the cusp region. There may or may not be a diurnal variation in ion escape flux from the cusp but the ENA escape flux can vary diurnally because of the variation in abundance of atomic oxygen encountered by the winter hemisphere cusp as it moves sunward and anti-sunward over the course of a day.

8. Conclusions

Based on the above data analysis and modeling results we state the following conclusion:

1. The fast atom (~1−300 eV) environment around the Earth consists of two components: a warm trapped oxygen component that may be associated with the geocorona (1−10 eV) and a hotter, escaping auroral zone component (10−300 eV).
2. The flux of the auroral zone component increases with increasing magnetic activity.
3. The winter hemisphere auroral zone emission rate varies diurnally during quiet times.
4. The mean energy of neutral atoms (in the 10-300 eV range) emitted from the earth increases with increasing magnetic activity.
5. During active intervals the auroral oval ENA emission region extends to higher altitudes.

9. References

Burch, J. L., Image mission overview, in *The IMAGE Mission*, edt. J. L. Burch, Kluwer Academic Publ., Dordrecht, The Netherlands, 2000.

Bisikalo, D. V., V. I. Shematovich, and J.-C. Gérard, A kinetic model of the formation of the hot oxygen geocorona 2. Influence of O^+ ion precipitation, *J. Geophys. Res.*, *100*, 3715, 1995.

Galand, M., and A. D. Richmond, Magnetic mirroring in an incident proton beam, *J. Geophys. Res.*, *104*, 4447, 1999.

Hickey, M. P., P. G. Richards, and D. G. Torr, New sources for the hot oxygen geocorona: Solar cycle, seasonal, latitudinal, and diurnal variations, *J. Geophys. Res.*, *100*, 17377, 1995.

Ishimoto, M., G. R. Romick and C.-I. Meng, Energy distribution of energetic O^+ precipitation into the atmosphere, *J. Geophys. Res.*, *97*, 8619, 1992.

Kan, J. R., and L. C. Lee, Energy coupling function and solar wind-magnetosphere dynamo, *Geophys. Res. Lett.*, *6*, 577, 1979.

Khan, H., M. R. Collier, and T. E. Moore, Case study of solar wind pressure variations and neutral atom emissions observed by IMAGE/LENA, *J. Geophys. Res.*, *108*(A12), 1422, doi:10.1029/2003JA009977, 2003.

Mitchell, D. G., et al., High energy neutral atom (HENA) imager for the IMAGE mission, in *The IMAGE Mission*, edt. J. L. Burch, Kluwer Academic Publ., Dordrecht, The Netherlands, 2000.

Moore, T. E., et al., The low energy neutral atom imager for IMAGE, in *The IMAGE Mission*, edt. J. L. Burch, Kluwer Academic Publ., Dordrecht, The Netherlands, 2000.

Moore, T. E., et al., Low energy neutral atoms in the magnetosphere, *Geophys. Res. Lett.*, *28*, 1143, 2001.

Peterson, W. K., H. L. Collin, A. W. Yau, and O. W. Lennartsson, Polar/toroidal imaging mass-angle spectrograph observations of suprathermal ion outflow during solar minimum conditions, *J. Geophys. Res.*, *106*, 6059, 2001.

Shematovich, V. I., D. V. Bisikalo, and J. C. Gérard, A kinetic model of the formation of the hot oxygen geocorona 1. Quiet geomagnetic conditions, *J. Geophys. Res.*, *99*, 23217, 1994.

Thomsen, M. F., J. E. Borovsky, R. M. Skoug, and C. W. Smith, Delivery of cold, dense plasma sheet material into the near-Earth region, *J. Geophys. Res.*, *108*(A4), 1151, doi:10.1029/2002JA009544, 2003.

Wilson, G. R., T. E. Moore, M. R. Collier, Low-energy neutral atoms observed near the Earth, *J. Geophys. Res.*, *108*(A4), 1142, doi:10.1029/2002JA009643, 2003.

Yau, A. W., W. K. Peterson, and E. G. Shelley, Quantitative parameterization of energetic ionospheric ion outflow, in *Modeling Magnetospheric Plasma*, edts. T. E. Moore and J. H. Waite, Jr., p. 211, AGU Monogr. Ser. 44, Washington, D.C., 1988.

Figure Captions

Figure 1. Spin-time LENA spectrograms for the two perigee passes that occurred on July 13, 2000. In the first (a) perigee occurred at 0010 UT and in the second (b) perigee occurred at 1424 UT. The dotted line is the nadir direction. The dash-dotted lines are the trailing (upper) and approaching (lower) limbs of the earth. The dashed line is the ram direction.

Figure 2. ACE solar wind data from July 12-13, 2000. In the top panel the Kan-Lee electric field is plotted and in the bottom panel is the dynamic pressure. The vertical dashed lines give the times of the first (a) and second (b) perigee passes of July 13th.

Figure 3. Spin-time LENA spectrograms for the second perigee pass of July 15, 2000. The format for this figure is the same as figure 1.

Figure 4. Average UVI auroral image from the time of the perigee pass shown in figure 3.

Figure 5. Here we divide the perigee pass images into a high latitude (MLat ≤ -55º) and low latitude group (MLat > -55º). In (a) we plot the diurnal variation of the integrated flux for the high latitude group and in (b) we plot the integrated flux of the low latitude group. In panels (c) and (d) are the variation with Ap of the integrated flux when the diurnal variation has been subtracted out.

Figure 6. Variation of the post-perigee integrated flux versus (a) the high latitude perigee integrated flux and (b) the low latitude perigee integrated flux. In each case the perigee integrated flux was corrected by subtracting its diurnal variation.

Figure 7. Variation of the post-perigee integrated flux with magnetic activity as measure by Ap.

Figure 8. Simulated LENA spin-time spectrograms for a source population that covers the earth below 950 km altitude. (a) The source temperature is 2 eV everywhere. (b) The source temperature has a background value of 2 eV that increases to 5 eV in the center of the auroral oval (65º MLat). (c) A source with a background temperature of 2 eV and an auroral oval temperature of 15 eV. (d) A source with a background temperature of 2 eV and an auroral oval temperature of 50 eV. The instrument had an assumed energy cutoff of 15 eV.

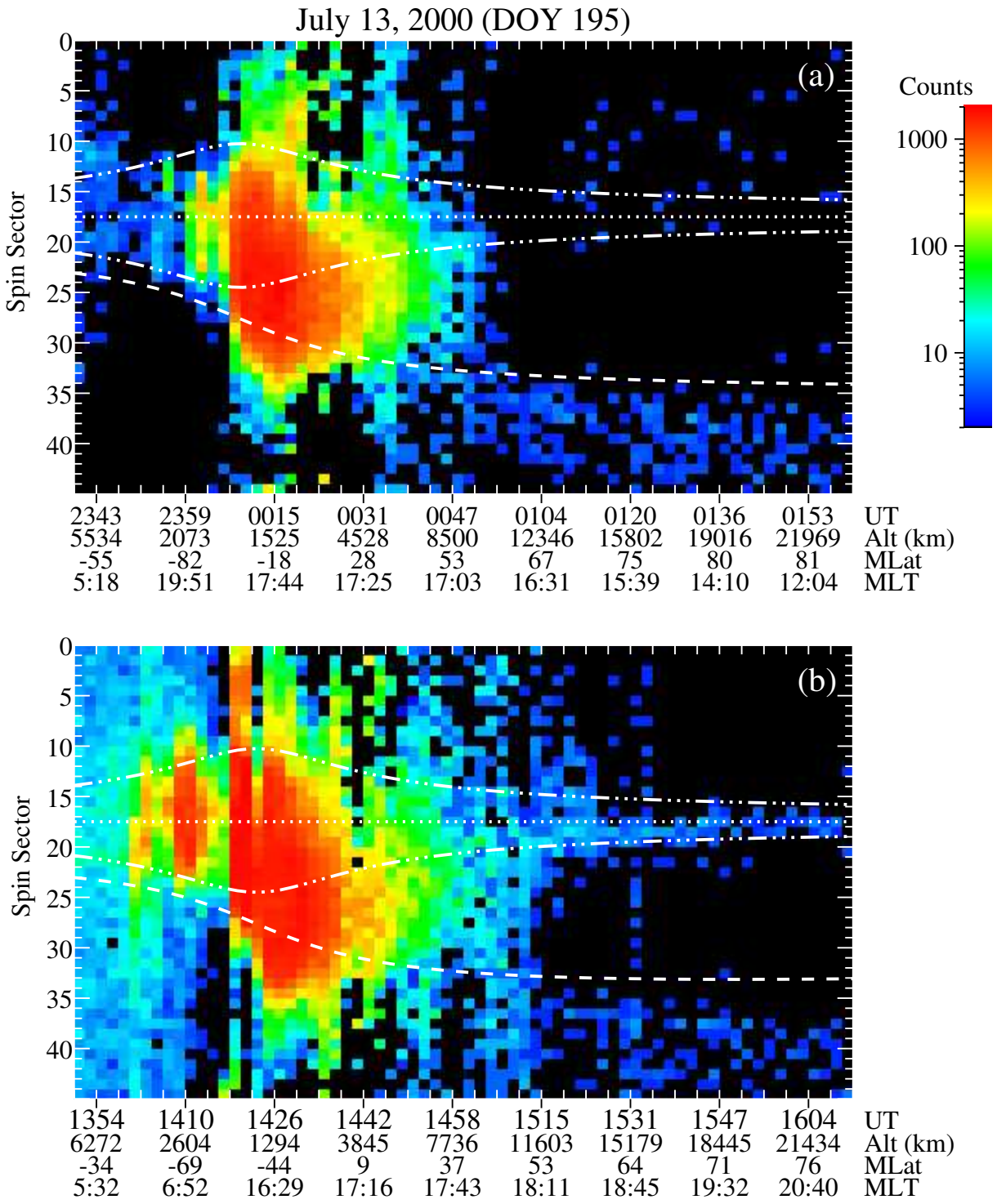
July 13, 2000 (DOY 195)
(a)
(b)
Spin Sector
Counts
1000
100
10
0
5
10
15
20
25
30
35
40
2343 2359 0015 0031 0047 0104 0120 0136 0153 UT
5534 2073 1525 4528 8500 12346 15802 19016 21969 Alt (km)
-55 -82 -18 28 53 67 75 80 81 MLat
5:18 19:51 17:44 17:25 17:03 16:31 15:39 14:10 12:04 MLT
1354 1410 1426 1442 1458 1515 1531 1547 1604 UT
6272 2604 1294 3845 7736 11603 15179 18445 21434 Alt (km)
-34 -69 -44 9 37 53 64 71 76 MLat
5:32 6:52 16:29 17:16 17:43 18:11 18:45 19:32 20:40 MLT

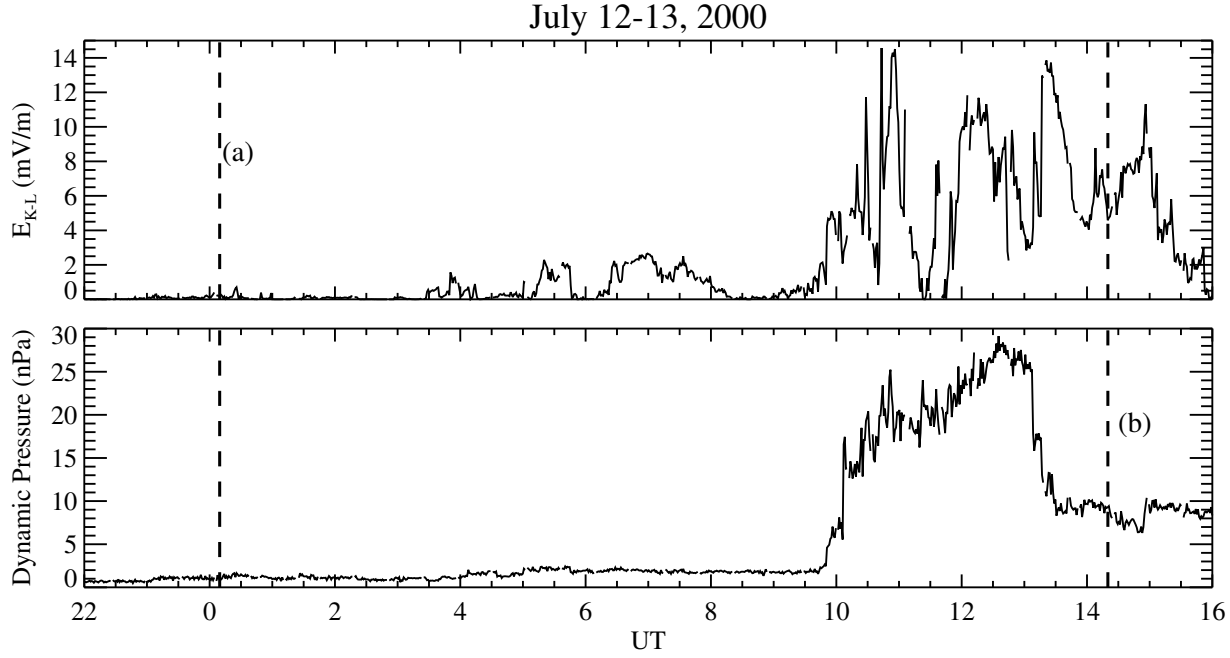
Time Shifted ACE Data
July 12-13, 2000
E_{K-L} (mV/m)
(a)
Dynamic Pressure (nPa)
(b)
UT
22
0
2
4
6
8
10
12
14
16

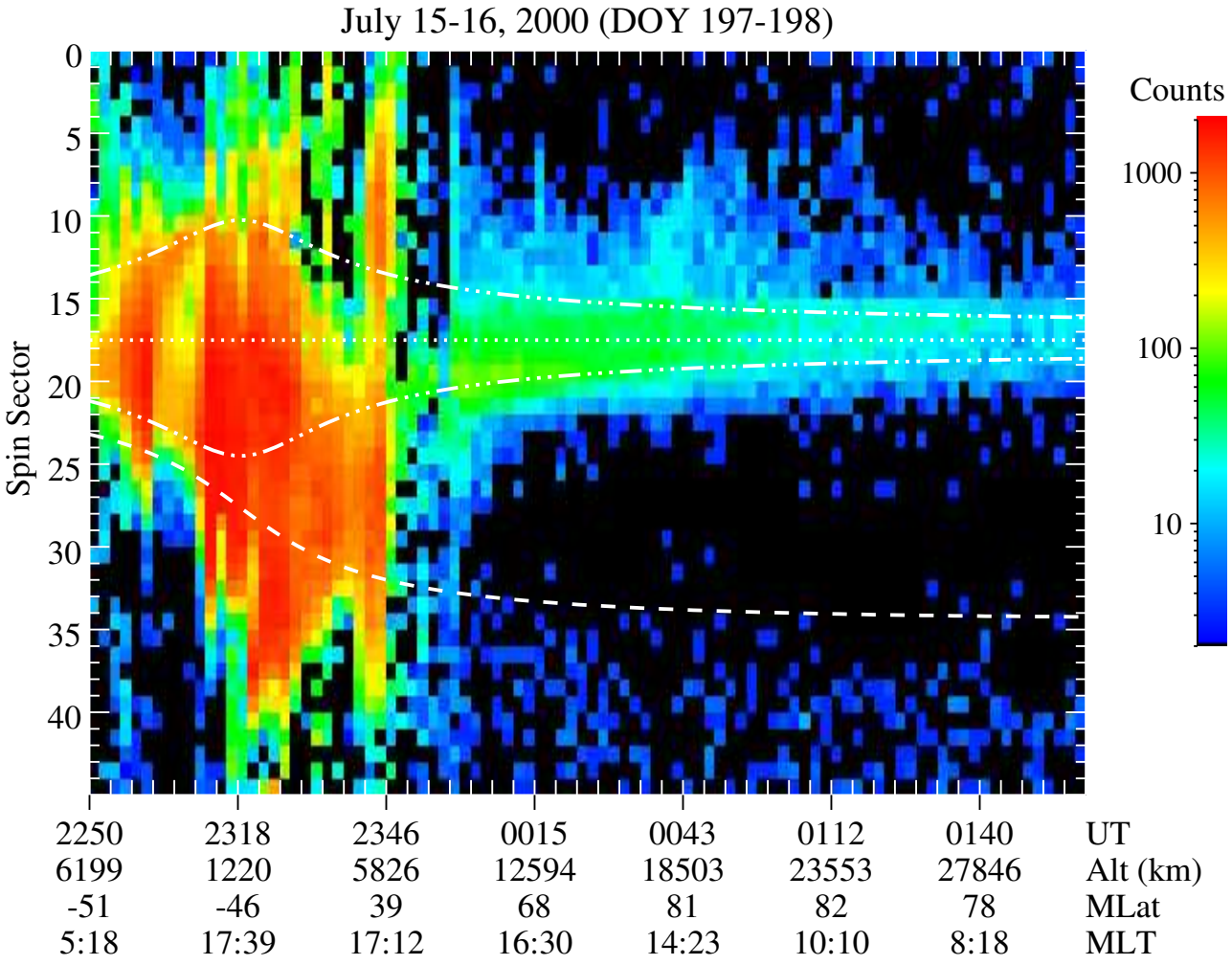
July 15-16, 2000 (DOY 197-198)
Spin Sector
0
5
10
15
20
25
30
35
40
Counts
1000
100
10
2250 2318 2346 0015 0043 0112 0140 UT
6199 1220 5826 12594 18503 23553 27846 Alt (km)
-51 -46 39 68 81 82 78 MLat
5:18 17:39 17:12 16:30 14:23 10:10 8:18 MLT

Average UVI LBHL Image

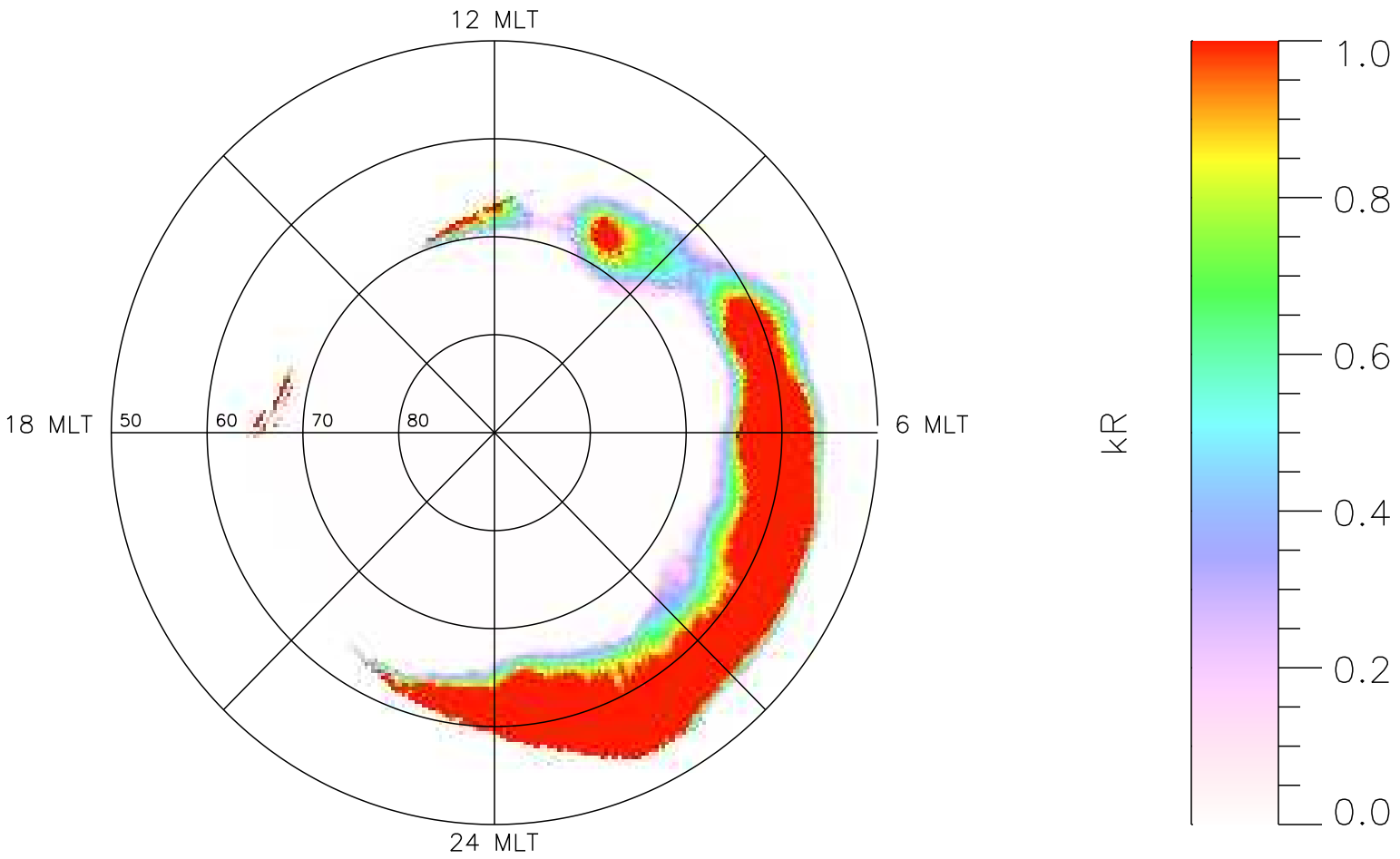

2000/07/15 22:50:14 – 23:26:25

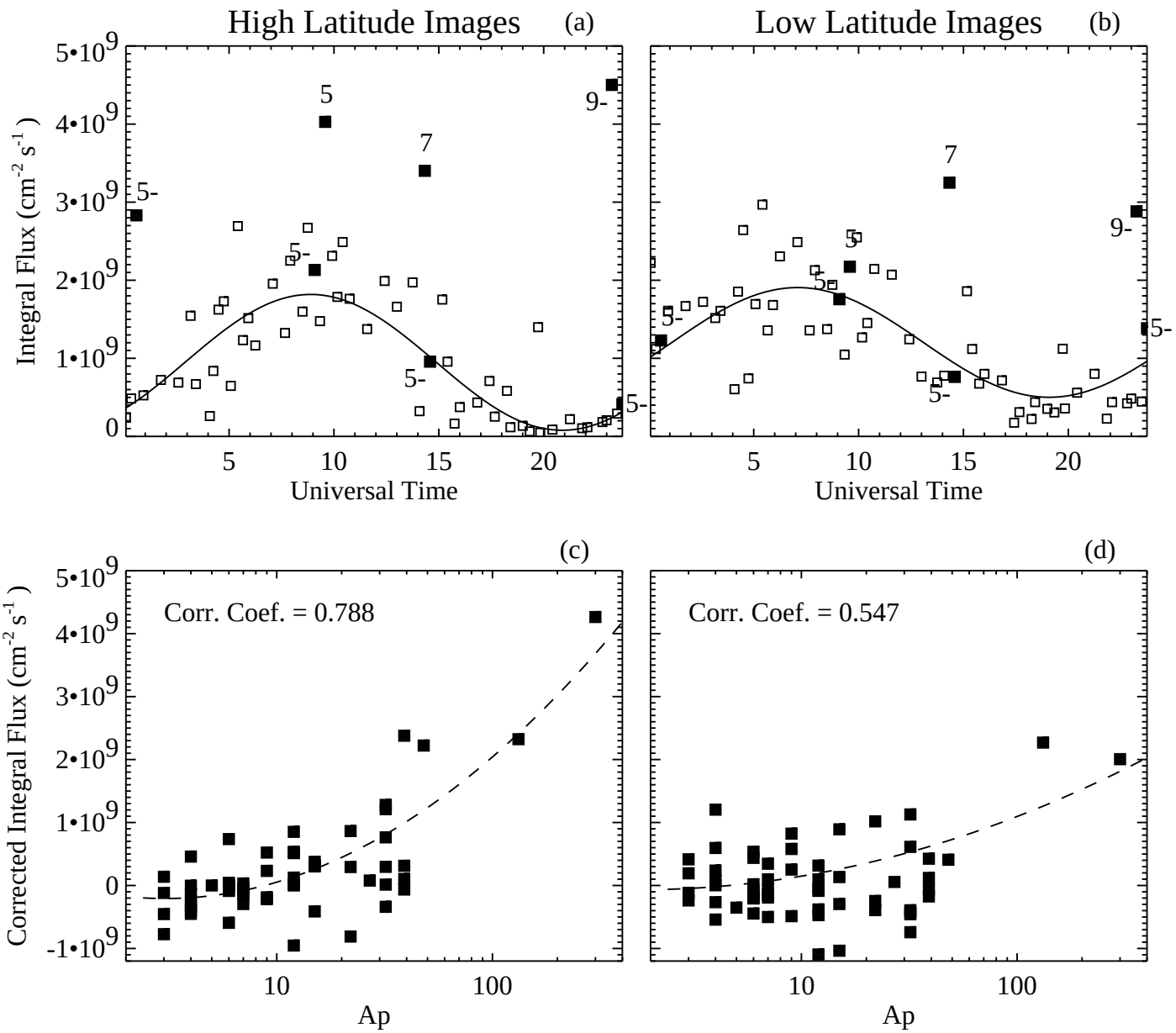
High Latitude Images
(a)
Low Latitude Images
(b)
Integral Flux (cm^{-2} s^{-1})
5•10^9
4•10^9
3•10^9
2•10^9
1•10^9
0
5
10
15
20
Universal Time
(c)
(d)
Corrected Integral Flux (cm^{-2} s^{-1})
Corr. Coef. = 0.788
Corr. Coef. = 0.547
-1•10^9
10
100
Ap

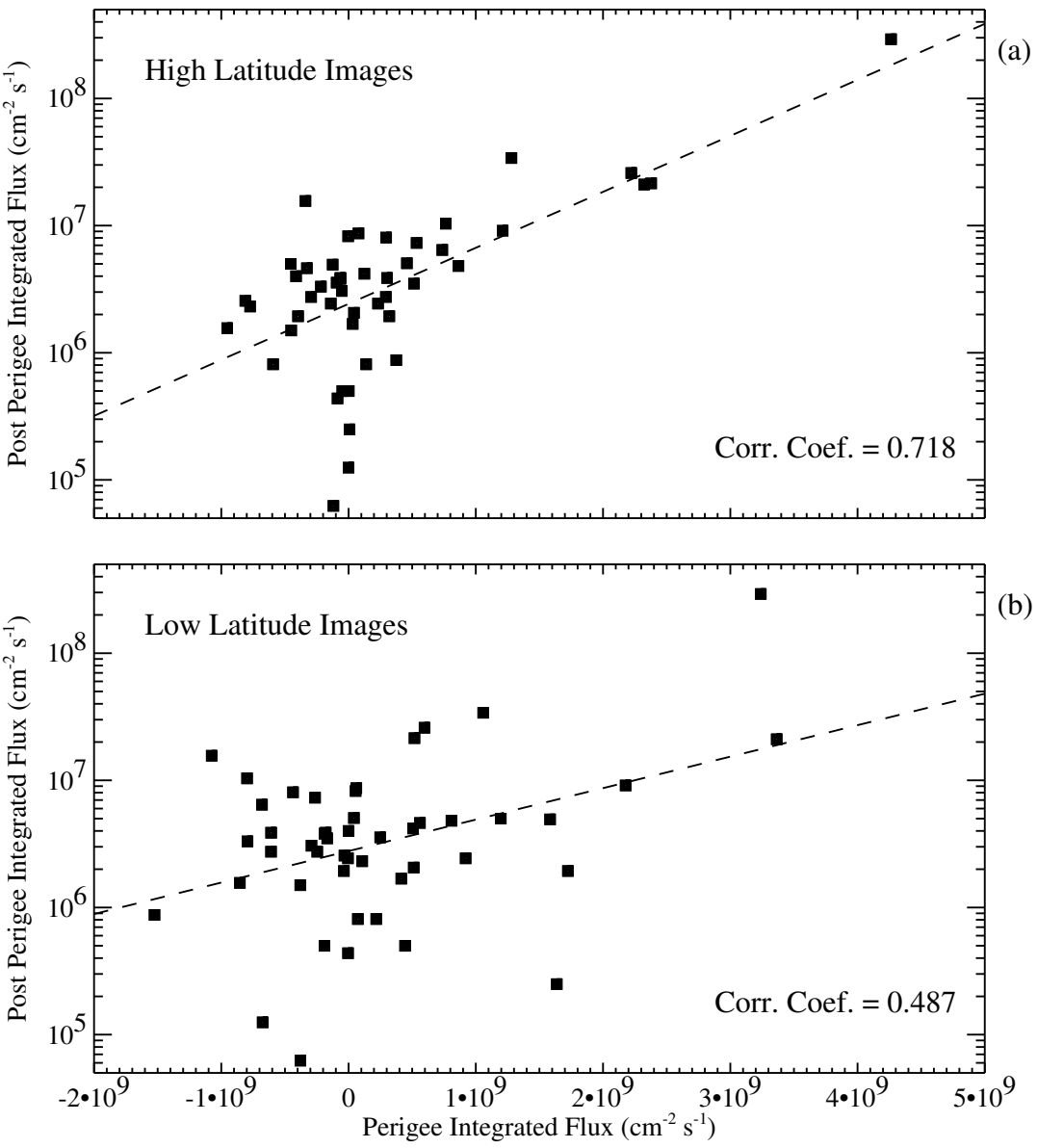
High Latitude Images
(a)
Post Perigee Integrated Flux (cm^{-2} s^{-1})
10^8
10^7
10^6
10^5
Corr. Coef. = 0.718
Low Latitude Images
(b)
Post Perigee Integrated Flux (cm^{-2} s^{-1})
10^8
10^7
10^6
10^5
Corr. Coef. = 0.487
-2•10^9
-1•10^9
0
1•10^9
2•10^9
3•10^9
4•10^9
5•10^9
Perigee Integrated Flux (cm^{-2} s^{-1})

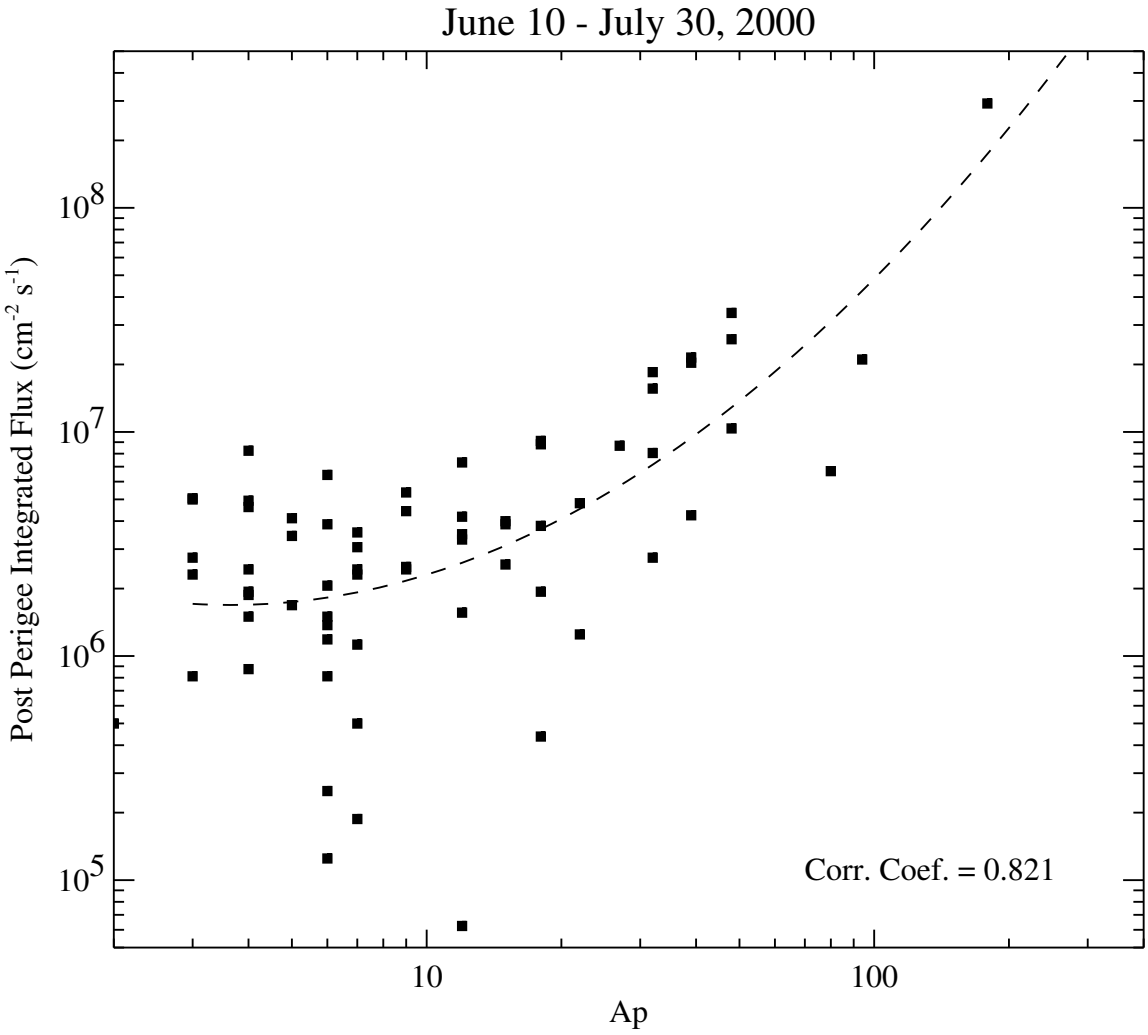
June 10 - July 30, 2000
Post Perigee Integrated Flux (cm-2 s-1)
10^8
10^7
10^6
10^5
10
100
Ap
Corr. Coef. = 0.821

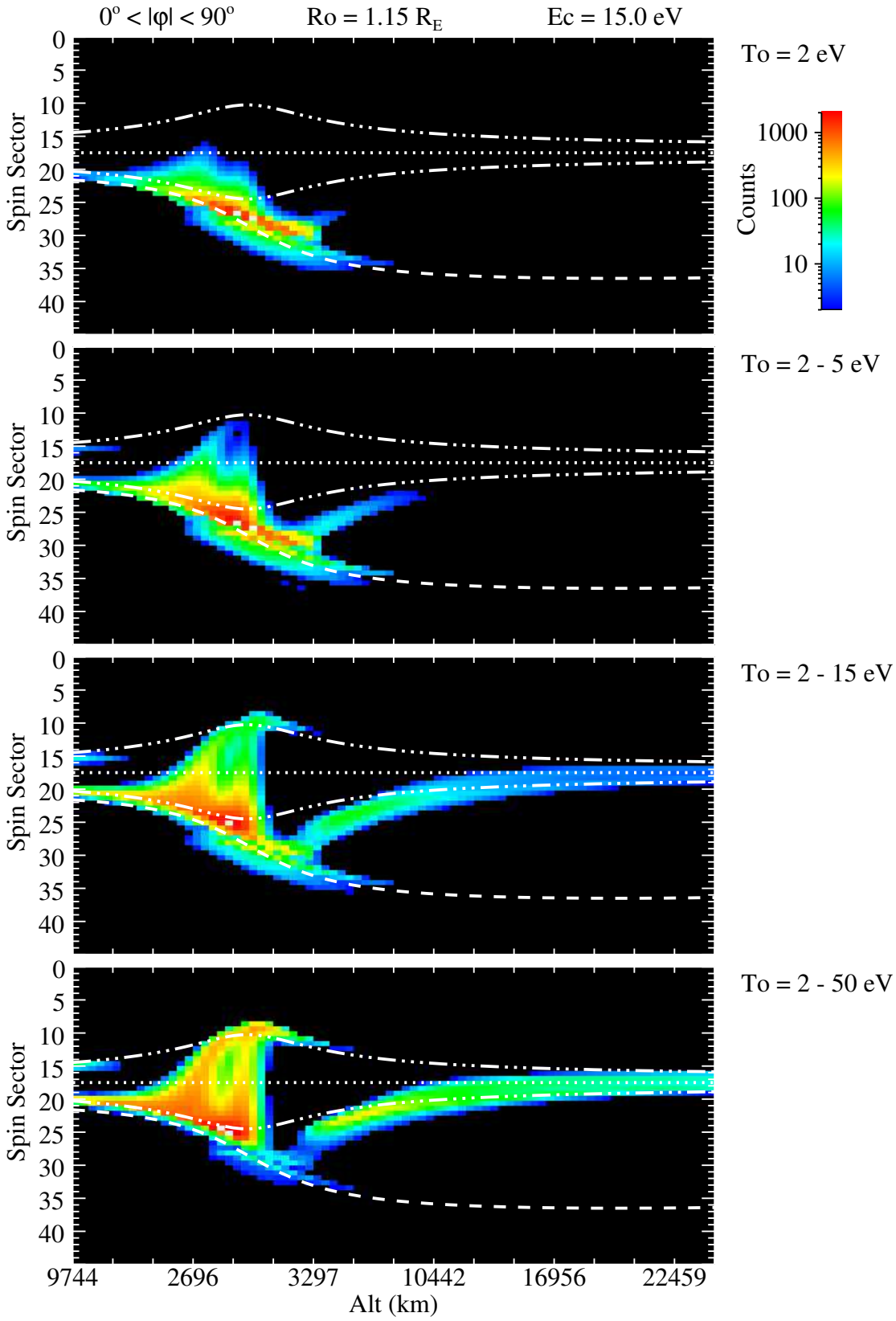
0° < |φ| < 90°
Ro = 1.15 R_E
Ec = 15.0 eV
To = 2 eV
To = 2 - 5 eV
To = 2 - 15 eV
To = 2 - 50 eV
Spin Sector
Counts
1000
100
10
0
5
10
15
20
25
30
35
40
9744
2696
3297
10442
16956
22459
Alt (km)